

Quasibound states of an antiproton and a hydrogen atom

Daniel Baye* and Jérémy Dohet-Eraly†

Physique Quantique, and

Physique Nucléaire Théorique et Physique Mathématique,

C.P. 229, Université libre de Bruxelles (ULB),

B-1050 Brussels, Belgium.

(Dated: November 26, 2019)

Abstract

Accurate three-body quantal calculations of the system composed of a proton, an antiproton, and an electron are performed in perimetric coordinates with the Lagrange-mesh method, an approximate variational calculation with the simplicity of a calculation on a grid. Quasibound states with respect to the $\bar{p} + \text{H}(n=2)$ threshold are obtained for $L = 60$ to 71 for various vibrational excitations. Their energies have accuracies up to about 10^{-14} atomic units while less precise energies are determined for $L = 56 - 59$ broader resonances. Their structure is analyzed with the help of mean distances between the particles. These mean distances indicate that the proton-electron subsystem is in excited states, mostly $n = 2$, as predicted by Sakimoto (Phys. Rev. A 98, 042503, 2018) with the Born-Oppenheimer approximation. A comparison performed with this approximation provides the accuracies of its energies and of its proton-antiproton mean distances.

* dbaye@ulb.ac.be

† jdoheter@ulb.ac.be

I. INTRODUCTION

The existence of low-energy antiproton beams allows the start of the realization of a long-awaited goal, the study of antimatter. Of particular interest is the simplest system, antihydrogen, which is now available in experiments [1]. It will allow testing a number of basic properties of antimatter [2]. Other systems involving antiprotons are very informative such as the hydrogenlike protonium [3, 4] or antiprotonic atoms where an antiproton replaces an electron. Among these atoms, antiprotonic helium composed of a helium nucleus, an antiproton, and an electron has been studied in very accurate experiments [5–7] and theoretical calculations [8–12]. Together, they provided a very precise measurement of the antiproton mass. Within the present experimental and theoretical error bars, this mass is found equal to the proton mass.

Antiprotonic helium presents a variation of structures with increasing angular momenta: successively hydrogenlike atom, quasistable pseudomolecule, and quasistable Rydberg pseudoatom [12]. An interesting question is what happens in such a system where the helium nucleus is replaced by a proton, i.e., the antiprotonic H^- ion. Because of the smaller charge of the proton, the existence of this antiproton-hydrogen system is far from obvious. In a study based on the Born-Oppenheimer approximation, Sakimoto has deduced that the binding of an antiproton by a hydrogen atom in its ground state is unlikely [13]. In a further work, however, he has shown that this binding could be possible at very high angular momenta when the hydrogen atom is in its first excited Stark-like state [14]. The reason is that the antiproton-hydrogen Born-Oppenheimer potential then has a much slower decrease than for hydrogen in its ground state and can be attractive enough at large distances. In a careful study of the decay processes, Sakimoto has shown that long-lived states could exist for total orbital momenta between 60 and 73.

The aim of the present paper is to establish the existence of these quasistable states of the proton-antiproton-electron system in a fully quantal three-body calculation. To this end, we employ the Lagrange-mesh method [15–20] in the perimetric coordinate system [21, 22], a numerical method with the simplicity of a mesh calculation and the accuracy of a variational calculation. This method does not require analytical evaluations of integrals and computer times remain reasonable. It is found accurate in a variety of spectroscopic or collision applications [20]. In particular, in the case of antiprotonic helium, the accuracy on

the energies matches the best available results in the literature and some other properties of the system can easily be computed [12].

The Lagrange-mesh method is briefly summarized in Sec. II and the conditions of the numerical calculations are determined. Energies and mean distances are presented in Sec. III. These results are compared with the Born-Oppenheimer approximation and discussed in Sec. IV. Section V contains a summary and a conclusion. Atomic units are used throughout.

II. THE LAGRANGE-MESH METHOD

A. Summary

We study the quantal three-body system formed by a proton of mass $m_p = 1836.152\,667\,5$, an antiproton of same mass $m_{\bar{p}} = m_p$, and an electron of mass $m_e = 1$ in atomic units, interacting only through Coulomb forces. Fine structure and relativistic effects are not taken into account.

The Schrödinger equation is solved in perimetric coordinates to avoid numerical problems with the singularities of the kinetic-energy operator and of the Coulomb interactions. The system of perimetric coordinates [21, 22] is defined by the three Euler angles ψ, θ, ϕ and the three coordinates

$$\begin{aligned} x &= r_{p\bar{p}} + r_{pe} - r_{\bar{p}e}, \\ y &= r_{p\bar{p}} - r_{pe} + r_{\bar{p}e}, \\ z &= -r_{p\bar{p}} + r_{pe} + r_{\bar{p}e}, \end{aligned} \tag{1}$$

involving the distances $r_{p\bar{p}}$, r_{pe} , and $r_{\bar{p}e}$ between the particles. The coordinates x, y and z vary over the $(0, \infty)$ interval. In perimetric coordinates, the Coulomb potential reads

$$V(x, y, z) = -\frac{2}{x+y} - \frac{2}{x+z} + \frac{2}{y+z}. \tag{2}$$

The kinetic energy operator for S states is given, e.g., in Ref. [23]. The general expression for arbitrary states can be found in Ref. [19].

The wave function with total orbital momentum L and natural parity $(-1)^L$ is expanded as [19]

$$\Psi_M^L = \sum_{K=0}^L \mathcal{D}_{MK}^L(\psi, \theta, \phi) \Phi_K^L(x, y, z). \tag{3}$$

where the $\mathcal{D}_{MK}^L(\psi, \theta, \phi)$ with $K \geq 0$ are parity-projected and normalized Wigner angular functions. In some cases, for $L > 0$, the sum can be truncated with excellent accuracy at some value K_{\max} . For $K_{\max} = 0$, the wave function presents a cylindrical symmetry along the $p\bar{p}$ axis. The value of K_{\max} gives information about the departure from this symmetry.

Let u_i , v_j , w_k be the zeros of Laguerre polynomials of respective degrees N_x , N_y , N_z , and h_x , h_y , h_z be three scale parameters with the dimension of a length in atomic units. The Lagrange-mesh method combines the three-dimensional mesh of $N_x N_y N_z$ points $(h_x u_i, h_y v_j, h_z w_k)$, a set of Lagrange functions $F_{ijk}^K(x, y, z)$ associated with each mesh point, and a Gauss quadrature consistent with this mesh [12, 15, 20]. The Lagrange functions are constructed from Laguerre polynomials and their exponential weight function. They verify the Lagrange conditions

$$F_{ijk}^K(h_x u_{i'}, h_y v_{j'}, h_z w_{k'}) \propto \delta_{ii'} \delta_{jj'} \delta_{kk'}, \quad (4)$$

i.e. each $F_{ijk}^K(x, y, z)$ vanishes at all mesh points except at the ijk point. These functions are normed at the Gauss quadrature approximation which is used everywhere. The $\Phi_K^L(x, y, z)$ functions in Eq. (3) are expanded in the Lagrange basis as

$$\Phi_K^L(x, y, z) = \sum_{i=1}^{N_x} \sum_{j=1}^{N_y} \sum_{k=1}^{N_z} C_{Kijk}^L F_{ijk}^K(x, y, z). \quad (5)$$

For each L value, the coefficients are given by the mesh equations

$$\sum_{K'jk} \left\{ \langle F_{i'j'k'}^{K'} | T_{K'K}^L | F_{ijk}^K \rangle + [V(h_x u_i, h_y v_j, h_z w_k) - E_{L\nu}] \delta_{KK'} \delta_{ii'} \delta_{jj'} \delta_{kk'} \right\} C_{Kijk}^L = 0, \quad (6)$$

where $T_{K'K}^L$ is the matrix element of the kinetic-energy operator between functions $\mathcal{D}_{MK'}^L$ and \mathcal{D}_{MK}^L . The matrix elements of operator $T_{K'K}^L$ between Lagrange functions are computed with the Gauss quadrature associated with the mesh [19]. The potential part in Eq. (6) is diagonal at this approximation because of the Lagrange property (4) while the kinetic-energy part has a tridiagonal block structure with many zeros in the blocks. The matrix of this system is thus rather sparse. Its size is $N_x N_y N_z (K_{\max} + 1)$. A limited number of eigenvalues of such big matrices can be obtained in rather short computing times with the code of Ref. [24]. The longest computations below with $K_{\max} = 3$ take about half an hour on a fast workstation. By increasing order, the *physical* eigenvalues $E_{L\nu}$ are labeled with the quantum number ν starting from zero. Other eigenvalues are discarded as explained below

in Sec. II B. The eigenvectors corresponding to physical eigenvalues provide, from Eqs. (5) and (3), square-integrable approximations of the wave functions.

This calculation is not variational for two reasons of different natures: (i) all eigenstates of $p\bar{p}e$ are unbound and (ii) the Gauss quadrature approximation is not exact. Nevertheless, some eigenvalues and eigenvectors of this system may provide approximate but accurate energies and eigenfunctions of quasibound states or narrow resonances. The difficulty is to isolate these eigenvalues from those corresponding to square-integrable approximations of continuum states. The separation of eigenvalues with a physical meaning is easily performed by computing the mean distances between the particles. For example, the mean distance between the proton and antiproton is simply given at the Gauss-quadrature approximation by

$$\langle r_{p\bar{p}} \rangle = \frac{1}{2} \sum_{Kijk} (C_{Kijk}^L)^2 (h_x u_i + h_y v_j). \quad (7)$$

Unphysical eigenvalues are indicated by very large electron-proton and electron-antiproton distances. Another consistent criterion is obtained from the probabilities

$$P_L(K) = \sum_{ijk} (C_{Kijk}^L)^2. \quad (8)$$

One observes that physical states always have $P_L(0)$ close to unity in contrast with approximations of continuum states. Because many channels are open below the energies we are looking for, it is important to have an idea of the energy domain where to search. This is provided by the Born-Oppenheimer results of Ref. [14]. They suggest the existence of quasibound states or narrow resonances in the domain $59 \leq L \leq 73$.

B. Conditions of the numerical calculations

The painful part of the calculation is to determine near-optimal values of seven parameters: h_x , h_y , h_z , N_x , N_y , N_z , and K . Once these choices have been made, it becomes easy to reproduce our calculations.

We have adopted the following strategy. First, since the system has a symmetry close to cylindrical, the Euler angles are chosen in such a way that the intrinsic axis 3 is chosen along the $p\bar{p}$ direction. With this convention, values of K can be limited to a small K_{\max} for the high accuracies presented below. Here, results are obtained with $K_{\max} = 3$ but there

is no difference with $K_{\max} = 2$ for $L \geq 68$. Second, the scale parameters h_x , h_y , h_z are selected. To this end, for each L , a number of calculations are performed with relatively small matrices where these parameters are varied to find plateaus of stability, i.e., regions such that small variations of these parameters do not affect a number of stable digits of the lowest quasibound eigenvalue ($\nu = 0$). These fast preliminary calculations were performed with $N_x = N_y = N_z = 20$ and $K_{\max} = 2$. As shown in Table I below, the parameters h_x , h_y , h_z need not be known with a high accuracy. They depend on the total orbital momentum L . Third, the best possible accuracy is searched for by increasing N_x , N_y , N_z . These values optimized on the second excited quasibound state ($\nu = 2$) are also given in Table I. Accurate results of the next excited states ($\nu = 3 - 5$) are obtained by increasing N_y only, up to 38.

The parameters are displayed in Table I. One observes that h_x and h_y monotonically increase with L . Parameter h_z is significantly larger and presents a minimum near $L = 65$. While N_x remains remarkably constant and rather small, N_y and N_z have contrasted evolutions. Above $L = 60$, N_y increases and N_z decreases. These tendencies are not valid below $L = 60$ because the smaller number of stable digits makes results poorly sensitive to the numbers of mesh points. Since the perimetric coordinates have no intuitive interpretation, the evolution of all these parameters is mainly phenomenological.

Table I. Parameters of the Lagrange meshes.

L	N_x	N_y	N_z	h_x	h_y	h_z
56	20	24	20	0.24	0.12	1.5
57	20	24	20	0.25	0.15	1.5
58	20	24	20	0.27	0.17	1.5
59	20	28	24	0.27	0.17	1.4
60	20	28	32	0.28	0.17	1.4
61	20	28	32	0.28	0.18	1.3
62	20	28	32	0.28	0.21	1.3
63	20	28	32	0.29	0.24	1.2
64	20	30	30	0.30	0.26	1.2
65	20	30	30	0.30	0.28	1.1
66	20	32	28	0.31	0.30	1.1
67	20	32	24	0.35	0.36	1.1
68	20	32	24	0.38	0.45	1.2
69	20	32	24	0.45	0.57	1.2
70	20	32	20	0.58	0.90	1.3
71	20	32	20	0.70	1.30	1.3
72	20	32	20	0.70	1.80	1.6

III. ENERGIES AND MEAN DISTANCES

Energies for $L = 56 - 72$ obtained from the three-body Schrödinger equation are presented in Table II. Their accuracies are based on the stability of digits when comparing calculations with (N_x, N_y, N_z) , $(N_x + 2, N_y, N_z)$, $(N_x, N_y + 2, N_z)$, and $(N_x, N_y, N_z + 2)$ mesh points. The last digit may be uncertain within a few units. Unexpectedly, the easiest calculation concern $L = 70$ where the matrix size $N_x N_y N_z (K_{\max} + 1)$ is smaller and the physical energies are easy to find because they are not mixed with other eigenvalues. For L smaller than about 60 – 62, on the contrary, the physical eigenvalues are mixed with many non-physical ones and their localization may require more efforts.

For each L value, the ground quasibound state and a number of its vibrational excited states are shown. When stability of an excited eigenvalue could not be reached, the location is left empty in the table. The number of stable digits gives a rough indication of the size of the width. In the antiprotonic helium case, it was observed that N stable decimal digits roughly correspond to a width $10^{-(N-1)}$ [12]. We expect that the same property holds here. Notice that, for eigenvalues with 14 stable digits, the width can even be smaller since this number of digits is limited by the computer accuracy.

The widths assumed here correspond to the decay of the $p\bar{p}e$ system into $p\bar{p} + e$ (Auger electron emission or autodetachment) and $\bar{p} + \text{H}$ (dissociation). According to Ref. [14], $\bar{p} + \text{H}$ dissociation is the main separation process. This is confirmed by the mean values of the distances between particles shown below. Notice however that the main decay channel according to Ref. [14] is due to spontaneous radiation, i.e., photon emission from the pe subsystem to the hydrogen ground state leading to a dissociation into $\bar{p} + \text{H}(1s)$. Let us recall that the structure of the pe subsystem is modeled as the lowest $n = 2$ Stark state in the Born-Oppenheimer study of Ref. [14]. The widths are found to be a little smaller than the radiative width of the $2p$ state of a free hydrogen atom. This radiative channel is absent in the present study and thus not included in the assumed width. Since the wave functions are available in a rather simple form, this channel could be studied in the present approach but is delayed to an ulterior work including other electromagnetic transitions.

From $L = 56$ to 59, the number of stable digits is small. The widths are expected to be large. No or few excited states could be obtained. They should be resonances too broad for the present static calculations. From $L = 60$ to 70, we display five vibrational excited states

Table II. Energies $E_{L\nu}$ of the lowest vibrational states as a function of L and ν .

L	$\nu = 0$	$\nu = 1$	$\nu = 2$
56	-0.15155		
57	-0.14774	-0.1453	
58	-0.144344	-0.14209	-0.1401
59	-0.14128113	-0.1393014	-0.13756
60	-0.1385388611	-0.13682153	-0.1353058
61	-0.13609647825	-0.13462534271	-0.13333407
62	-0.133936537967	-0.13269402621	-0.1316112327
63	-0.132043690689	-0.13101194704	-0.13012040959
64	-0.1304040491368	-0.129565256171	-0.12884774188
65	-0.1290048721099	-0.128341265648	-0.12778054460
66	-0.12783435033022	-0.1273280835826	-0.126906785039
67	-0.1268814293332	-0.1265142967803	-0.12621463030
68	-0.12613558871367	-0.1258885427503	-0.12569184978
69	-0.12558636854493	-0.12543866774143	-0.12532474227
70	-0.12522187107221	-0.12514963712438	-0.125095923153
71	-0.12502315145032	-0.12499811020158	-0.1249800756
72	-0.12494845876	-0.12494320	-0.1249392
L	$\nu = 3$	$\nu = 4$	$\nu = 5$
58	-0.1383		
59	-0.13599	-0.13464	
60	-0.1339698	-0.132798	-0.13176
61	-0.132203567	-0.13121623	-0.13035704
62	-0.1306702054	-0.129854541	-0.12914931
63	-0.1293523321	-0.128692500	-0.128127166
64	-0.1282359709	-0.1277159374	-0.127275102
65	-0.1273084143	-0.126912127	-0.126580404
66	-0.1265574681	-0.1262687282	-0.12603061
67	-0.1259708842	-0.1257731515	-0.125613008
68	-0.12553565717	-0.1254118104	-0.125313632
69	-0.125236885915	-0.1251619068	-0.12511661
70	-0.1250558121336	-0.1250257350	-0.12500309

(see Sec. IV for a justification of this interpretation). The states become narrower when L increases and broader when ν increases. For $L = 70$, the $\nu = 5$ energy is very close to the $\bar{p} + \text{H}(n = 2)$ dissociation threshold. This excited vibrational state is probably the highest to be quasibound. For $L = 71$, only the $\nu = 0$ state is quasibound. We display the energies of the first two resonances which are extremely narrow. No quasibound state is found for $L = 72$ but the ground-state resonance is also very narrow.

The binding energies $-E_{L\nu} - 1/8$ with respect to the $\bar{p} + \text{H}(n = 2)$ dissociation threshold are displayed in logarithmic scale in Fig. 1. One observes that they decrease monotonically,

faster than exponentially, as a function of L . For each L value except for $L \geq 70$, the points in the figure present an almost constant spacing. This corresponds to exponentially decreasing binding energies as a function of ν in the considered range $\nu \leq 5$.

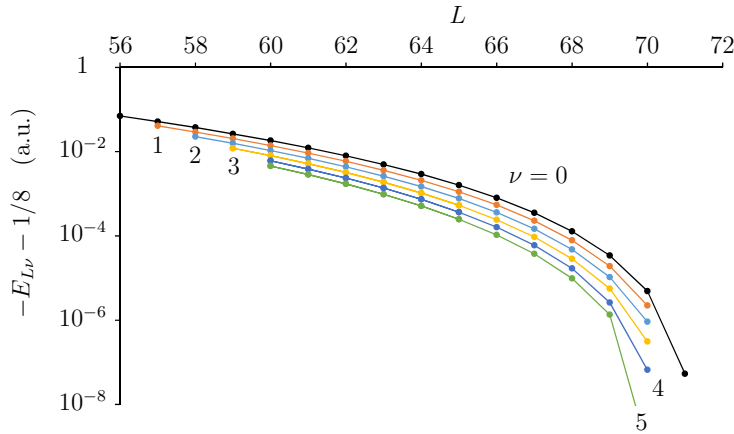


Figure 1. Binding energies $-E_{L\nu} - 1/8$ with respect to the $\bar{p} + \text{H}(n = 2)$ threshold as a function of L . The curves are labeled by the vibrational quantum number ν .

In Table III are presented mean values of the distances $\langle r_{p\bar{p}} \rangle$ between proton and antiproton, $\langle r_{pe} \rangle$ between proton and electron, and $\langle r_{\bar{p}e} \rangle$ between antiproton and electron. Here also, only stable digits are kept except the last one which may be uncertain within a few units. The number of presented decimal digits is limited to a maximum of seven. In all cases, the accuracy does not exceed 9 decimal places in the range $65 - 70$. Indeed, since the method is approximately variational, an error ϵ on wave functions and mean values corresponds to an error of about ϵ^2 on energies. A 10^{-9} accuracy on the distances means that the accuracy of the energies in this range could be better than 10^{-14} .

Let us first consider $\langle r_{pe} \rangle$. This mean distance decreases monotonically from the large value 12.5 at $L = 56$ to 5.65 at $L = 71$ (see also Fig. 2). It decreases when ν increases. Around $L = 69$, $\langle r_{pe} \rangle$ is very close to 6, i.e., the mean distance between the proton and electron of a free hydrogen atom in an $n = 2$ state. This nicely corresponds to the assumption in the model of Ref. [14]. For lower L values, higher excitations of hydrogen also play a role. Beyond $L = 69$ and for some higher vibrational states, a significant component of hydrogen in its ground state must also be present.

Let us now turn to the proton-antiproton mean distance $\langle r_{p\bar{p}} \rangle$. It monotonically increases with both L and ν . The increase with L follows from the centrifugal effect. The increase with

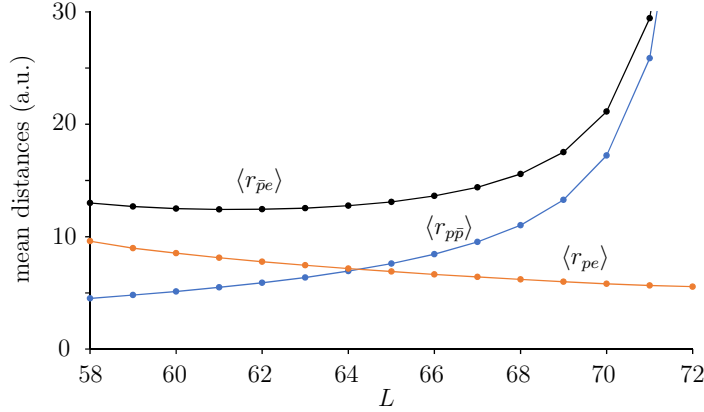


Figure 2. Mean distances $\langle r_{p\bar{p}} \rangle$, $\langle r_{pe} \rangle$, and $\langle r_{\bar{p}e} \rangle$ between the particles for $\nu = 0$.

ν corresponds to a broadening due to vibrational excitation. This is discussed in another way in Sec. IV.

The antiproton-electron mean distance $\langle r_{\bar{p}e} \rangle$ is always larger than the proton-electron one $\langle r_{pe} \rangle$ as expected from the electrostatic repulsion between these particles. It also increases with the vibrational quantum number ν .

As mentioned before, the probabilities of K components give indications about the cylindrical symmetry of the system. The $K > 0$ probabilities are displayed with a maximum of ten decimal digits in Table IV and illustrated by Fig. 3. They are quite inaccurate for $L < 60$. For $L > 65$, an excellent accuracy on the energies is already obtained with $K_{\max} = 2$, or even $K_{\max} = 1$ for $L \geq 70$. On the contrary, for $L < 60$, values larger than 3 could be necessary in more elaborate calculations of resonance properties.

Table IV shows contrasting behaviors for the probabilities $P_{L\nu}(K)$ of vibrational excited states. For $K = 1$, the probabilities decrease when ν increases. For $K = 2$, they increase for $L < 66$ and decrease for $L > 66$. For $K = 3$, they always increase with ν . The dependence of $P_{L0}(K)$ on L is illustrated in Fig. 3. All probabilities decrease monotonically with L . The $K = 1$ probabilities are the largest. The $K = 2$ probabilities are smaller than 10^{-4} . The $K = 3$ probabilities become smaller than 10^{-11} beyond $L = 68$. They explain why this component does affect the energies in this range. The smallness of the $K > 0$ probabilities implies that $P_{L\nu}(0)$ is always close to unity. Its smallest value, near 0.92, is for $L = 56$.

Table III. Mean distances between the particles as a function of L and ν .

L	ν	$\langle r_{p\bar{p}} \rangle$	$\langle r_{pe} \rangle$	$\langle r_{\bar{p}e} \rangle$
56	0	3.96	12.5	15.4
57	0	4.23	10.6	13.8
	1	4.5		
58	0	4.504	9.6	13.0
	1	4.7		
59	0	4.80035	8.985	12.677
	1	5.208	8.82	12.88
	2	5.6		
60	0	5.12423	8.5280	12.5026
	1	5.5792	8.266	12.650
	2	6.06	8.1	13.0
61	0	5.4865215	8.127147	12.421703
	1	5.993173	7.87762	12.62937
	2	6.5430	7.6553	12.9061
62	0	5.897680	7.77372	12.43425
	1	6.465661	7.54210	12.71805
	2	7.085388	7.32942	13.07158
63	0	6.3720818	7.4546917	12.5407382
	1	7.0153989	7.2428201	12.9163477
	2	7.7208651	7.049496	13.3718622
64	0	6.9301622	7.1637094	12.7541037
	1	7.6689101	6.9717212	13.2414497
	2	8.4837312	6.7978713	13.8224752
65	0	7.6027009	6.8961919	13.0991423
	1	8.4665215	6.7237866	13.7271771
	2	9.425775	6.5691080	14.468225
66	0	8.4389209	6.6486442	13.6196868
	1	9.4736262	6.4955777	14.4335341
	2	10.63183	6.359864	15.388694
67	0	9.5236837	6.4183166	14.3951181
	1	10.804703	6.2846998	15.4698911
	2	12.251974	6.1681192	16.729417
68	0	11.018548	6.2031032	15.5807073
	1	12.680887	6.0897259	17.0520249
	2	14.578629	5.9930624	18.778600
69	0	13.275801	6.0018471	17.5208472
	1	15.588816	5.9106846	19.6608992
	2	18.25717	5.8355943	22.17830
70	0	17.221213	5.8160442	21.1321144
	1	20.798740	5.7508863	24.5630015
	2	24.959507	5.6997582	28.601044
71	0	25.884281	5.6568797	29.4453979
	1	32.344848	5.6214789	35.802946
	2	39.9390	5.594804	43.3144
72	0	50.412	5.554296	53.669

Table IV. Probabilities $P_{L\nu}(K)$ of the $K > 0$ components as a function of L and ν .

L	ν	$P_{L\nu}(K = 1)$	$P_{L\nu}(K = 2)$	$P_{L\nu}(K = 3)$
56	0	0.082		
57	0	0.047	0.003	
58	0	0.031	0.0006	
59	0	0.02162	0.000179	0.000003
	1	0.024	0.0008	
60	0	0.015677	0.0000841	0.0000031
	1	0.01551	0.000136	0.000003
	2	0.0169	0.0009	
61	0	0.011536186	0.000033516	0.000000104
	1	0.0110244	0.0000512	0.00000034
	2	0.01050	0.00010	0.000010
62	0	0.0085988	0.0000161	0.00000003
	1	0.0080172	0.00002199	0.00000007
	2	0.0074112	0.00002714	0.00000013
63	0	0.0064633290	0.0000078829	0.0000000085
	1	0.0059116281	0.0000098772	0.0000000174
	2	0.00536622	0.000011321	0.0000000274
64	0	0.0048875929	0.0000038902	0.0000000026
	1	0.004401258	0.0000045151	0.0000000047
	2	0.003939311	0.0000048635	0.0000000067
65	0	0.0037101822	0.0000019199	0.0000000008
	1	0.0032987199	0.0000020724	0.0000000013
	2	0.002920324	0.0000021061	0.0000000017
66	0	0.0028202995	0.0000009394	0.0000000002
	1	0.002482245	0.0000009447	0.0000000003
	2	0.002179932	0.0000009064	0.0000000004
67	0	0.0021402927	0.0000004505	0.0000000001
	1	0.0018698693	0.0000004224	0.0000000001
	2	0.0016343534	0.0000003824	0.0000000001
68	0	0.0016148758	0.0000002080	0.0000000000
	1	0.0014052474	0.0000001819	0.0000000000
	2	0.0012276417	0.0000001553	0.0000000000
69	0	0.0012044099	0.0000000895	0.0000000000
	1	0.0010494638	0.0000000732	0.0000000000
	2	0.000922250	0.0000000590	0.0000000000
70	0	0.0008816009	0.0000000338	0.0000000000
	1	0.0007769888	0.0000000260	0.0000000000
	2	0.000694041	0.0000000199	0.0000000000
71	0	0.0006344935	0.0000000099	0.0000000000
	1	0.0005759509	0.0000000073	0.0000000000
	2	0.0005303019	0.0000000054	0.0000000000
72	0	0.000474112	0.0000000020	0.0000000000

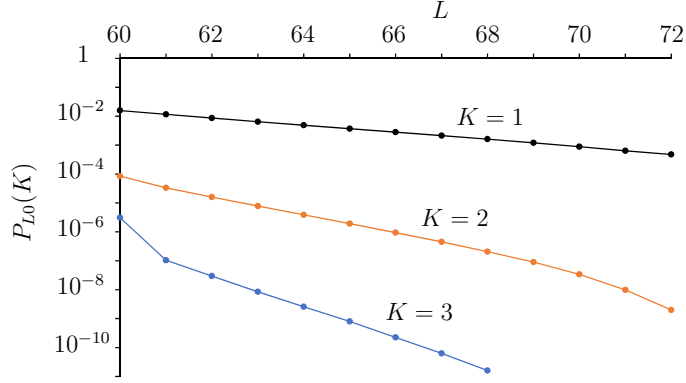


Figure 3. Probabilities of the $K > 0$ components as a function of L for $\nu = 0$.

IV. DISCUSSION

The electron emission energies $E_{L0} - E_{p\bar{p}}^{L-l}$, where $E_{p\bar{p}}^{L-l}$ is the highest $p\bar{p}$ threshold energy below E_{L0} corresponding to the lowest orbital momentum l of the emitted electron, are displayed in Fig. 4 as a function of L . The points are labeled with the value of this minimal orbital momentum l (denoted as l_0 in Table II of Ref. [14]). One observes that this energy is very small at $L = 59$, which may explain why the search for optimal parameters was very difficult in that case. It is also quite small for $L = 56$ and 61. These energies tend to more constant values at high L , including for the $L = 72$ narrow resonance.

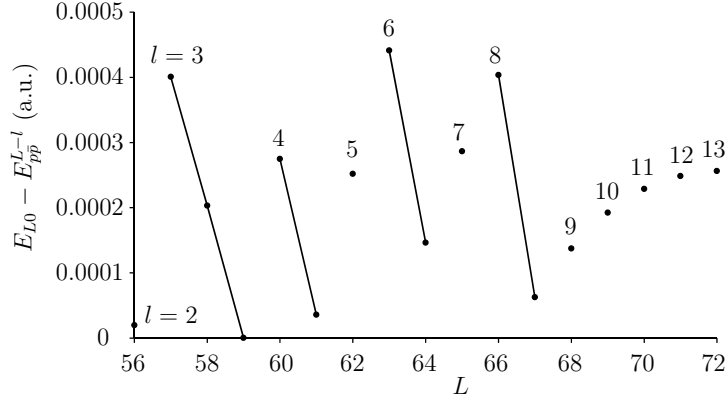


Figure 4. Electron emission energy $E_{L0} - E_{p\bar{p}}^{L-l}$ for the lowest electron orbital momentum l as a function of L , where $E_{p\bar{p}}^{L-l}$ is the energy of the highest open threshold below E_{L0} .

The states from $L = 60$ to 71 have long lifetimes with respect to the channels $p\bar{p} + e$ because this Auger electron emission (or autodetachment) is a slow process. The spontaneous emission of an electron is strongly hindered in these states because the electron can only be emitted with a rather high orbital momentum $l \geq 3$ [14, 25]. The same effect explains the long lifetimes of some levels of antiprotonic helium (Ref. [12] and references therein). The large number of stable digits indicates that all couplings with continuum states are weak in this range of L values in agreement with the findings of Ref. [14]. This is also confirmed by the absence or small number of non-physical eigenvalues among the physical energies in this domain.

The quantum number ν is interpreted here as representing a vibrational excitation. In order to deepen this interpretation, we now perform a comparison with the Born-Oppenheimer picture as used in Ref. [14]. To this end, we solve the Born-Oppenheimer equation

$$\left(-\frac{1}{2}\Delta - \frac{1}{r_{pe}} + \frac{1}{r_{\bar{p}e}} - \frac{1}{R}\right)\chi_{nm}(\mathbf{r}_{pe}, R) = \mathcal{E}_{nm}(R)\chi_{nm}(\mathbf{r}_{pe}, R), \quad (9)$$

where $R \equiv r_{p\bar{p}}$ is fixed and the Laplacian Δ corresponds to the proton-electron coordinate \mathbf{r}_{pe} . The energies depend on the parameter R and on the magnetic quantum number m . They are labeled by the excitation quantum number n starting from 0. This equation is separable in confocal elliptic coordinates (or prolate spheroidal coordinates) [26]. Here, we solve it for $m = 0$ with the Lagrange-mesh method as explained in Ref. [27].

For the coordinate $\xi = (r_{pe} + r_{\bar{p}e})/R - 1$ defined in the interval $(0, \infty)$, a Lagrange-Laguerre mesh with N_ξ points and a scale parameter h is employed. For the coordinate $\eta = (r_{pe} - r_{\bar{p}e})/R$ defined in the interval $(-1, 1)$, a Lagrange-Legendre mesh with N_η points is used. For $m = 0$, the azimuthal angle φ of \mathbf{r}_{pe} does not play a role. Since the calculation is very fast, a rough optimization is sufficient. We use $N_\xi = 30$ and $N_\eta = 20$. The scale parameter is given by $h = \max(6/R - 1, 2/R)$. The lowest energies $\mathcal{E}_{00}(R)$ correspond to those labeled (0,0,0) in Refs. [14, 26]. The first excited ones $\mathcal{E}_{10}(R)$ correspond to those labeled (1,0,0) in these references. These energies are obtained with at least nine stable decimal digits. When rounded at the fifth decimal digit, they perfectly agree with the results of Ref. [26].

The energies $\mathcal{E}_{10}(R)$ are then used as a proton-antiproton potential in radial Schrödinger equations with reduced mass $m_p/2$. These equations are solved for $L = 58$ to 71 with the Numerov algorithm. Above $R = 2$, the steps 0.1, 0.05, and 0.02 have been used up to

Table V. Born-Oppenheimer energies $E_{L\nu}^{BO}$ and mean distances $\langle R \rangle_{L\nu}$ of the lowest vibrational states as a function of L .

L	E_{L0}^{BO}	$\langle R \rangle_{L0}$	E_{L1}^{BO}	$\langle R \rangle_{L1}$	E_{L2}^{BO}	$\langle R \rangle_{L2}$
58	-0.1439567	4.5952	-0.1417104	4.9849	-0.1397098	5.4040
59	-0.1409907	4.8804	-0.1390290	5.3055	-0.1372899	5.7638
60	-0.1383227	5.1987	-0.1366258	5.6654	-0.1351293	6.1703
61	-0.1359388	5.5575	-0.1344874	6.0739	-0.1332150	6.6349
62	-0.1338256	5.9669	-0.1326009	6.5440	-0.1315350	7.1736
63	-0.1319704	6.4413	-0.1309544	7.0937	-0.1300774	7.8091
64	-0.1303614	7.0012	-0.1295362	7.7496	-0.1288310	8.5753
65	-0.1289873	7.6779	-0.1283352	8.5528	-0.1277847	9.5246
66	-0.1278375	8.5217	-0.1273408	9.5701	-0.1269278	10.7438
67	-0.1269017	9.6198	-0.1265423	10.9188	-0.1262493	12.3869
68	-0.1261701	11.1386	-0.1259291	12.8271	-0.1257375	14.7552
69	-0.1256327	13.4434	-0.1254894	15.7992	-0.1253790	18.5175
70	-0.1252778	17.5009	-0.1252083	21.1596	-0.1251568	25.4150
71	-0.1250861	26.4883	-0.1250624	33.1343	-0.1250453	40.9531

$R = 100$. Below $R = 2$, these high L effective potentials are approximated only by the centrifugal barriers. The results are displayed in Table V for $h = 0.02$. The energies $E_{L\nu}^{BO}$ of the three calculations agree within at least 7 decimal digits for the three lowest vibrational states. This accuracy is better than the difference between the present energies and the energies E_{BO} of the first column of Table II in Ref. [14] which are based on interpolations of the results of Ref. [26]. For the mean proton-antiproton distances, an absolute accuracy better than about 10^{-5} is obtained with $h = 0.02$ for $\nu = 0$ and a little less good for $\nu = 1$ and 2. The accuracy is poorer for $L = 71$. For this L value, the existence of vibrational excited states below the $\bar{p} + \text{H}(n = 2)$ threshold in the Born-Oppenheimer approach is in contradiction with the three-body results.

In Fig. 5, we display for $\nu = 0 - 2$ the differences of the energies $E_{L\nu}^{BO}$ of Table V computed with the Born-Oppenheimer approach and the quantal three-body energies $E_{L\nu}$

of Table II. These differences monotonically decrease. They are positive below $L = 65 - 66$ and negative above. They also decrease with increasing ν . A figure involving the improved Born-Oppenheimer energies of the second column of Table II in Ref. [14] would be hardly different at the present scale. The error of the Born-Oppenheimer approximation is always smaller than 4×10^{-4} atomic units. This good agreement confirms the interpretation of ν as a vibrational quantum number.

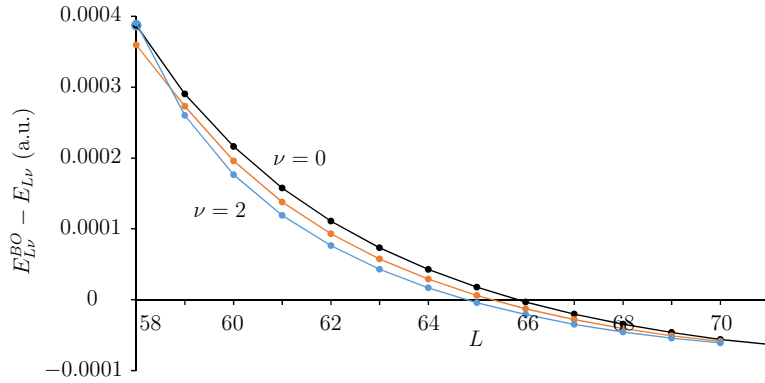


Figure 5. Differences of the energies $E_{L\nu}^{BO}$ of Table V computed at the Born-Oppenheimer approximation and the three-body energies $E_{L\nu}$ of Table II for $L = 58 - 71$ and $\nu = 0 - 2$.

This picture is also confirmed by the ratios of mean distances $\langle R \rangle_{L\nu}$ of Table V obtained at the Born-Oppenheimer approximation and the quantal mean distances $\langle r_{p\bar{p}} \rangle_{L\nu}$ of Table III. With the exception of $L = 71$ for which only one quantal state is below the $\bar{p} + H(n = 2)$ threshold, the Born-Oppenheimer mean distances are between one and two percent larger than the quantal ones. This is true for the three presented ν values. For $L = 71$, the $\nu = 0$ ratio is smaller than unity, i.e., 0.9815.

Finally, let us mention that we found some evidence around $L = 65$ for other resonances with fewer stable digits and with mean proton-electron distances close to 3. These resonances would correspond to configurations with a hydrogen atom mainly in its ground state. Such structures would contradict the Born-Oppenheimer picture of possible structures discussed in Ref. [14]. Unfortunately, since these resonances should be broader, the present approach is not adequate for confirming their existence and evaluating their properties.

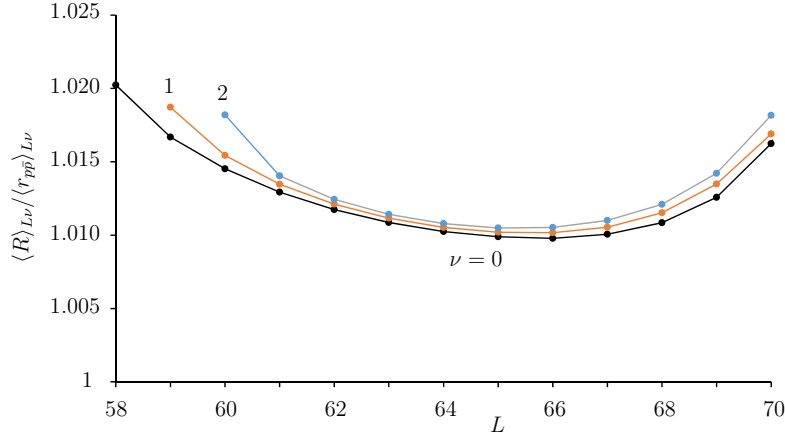


Figure 6. Ratios of mean distances $\langle R \rangle_{L\nu}$ of Table V computed at the Born-Oppenheimer approximation to the corresponding mean distances $\langle r_{p\bar{p}} \rangle_{L\nu}$ of Table III for $L = 58 - 70$ and $\nu = 0 - 2$.

V. CONCLUSION

With an accurate three-body, approximately variational, calculation on a Lagrange mesh, we establish the existence of quasibound states below the $\bar{p} + \text{H}(n = 2)$ threshold with extremely small widths for spontaneous dissociation. The existence of these states was predicted in the Born-Oppenheimer study of Ref. [14]. We show that several narrow vibrational states exist over a range of L values. We have studied the six lowest vibrational states between $L = 60$ and 70 and the only existing such state at $L = 71$. Below $L = 60$, rather narrow resonances still exist but are less well described by the present static study. In all cases, the corresponding configurations are not far from a cylindrical symmetry around the proton-antiproton axis.

This vibrational interpretation is confirmed by a Born-Oppenheimer calculation similar to the one performed in Ref. [14]. The accuracy of this approximation in the present case is thus determined. It is found to improve with increasing L , reaching about 10^{-4} atomic units for the energies.

Accurate values are also obtained for the three mean distances between the particles. The mean distances between the proton and electron indicate that the hydrogen-atom-like substructure in the three-body system is in a superposition of excited states, sometimes dominated by the $n = 2$ state assumed in Ref. [14]. The proton-antiproton mean distances increase as expected from the centrifugal effect. They are well described by the Born-Oppenheimer approximation with an overestimation between 1 and 2 percents.

The number of stable digits obtained for the energies gives indications about the widths of the quasibound states which are found very small between $L = 60$ and 71 . These widths only correspond to spontaneous dissociations into $p\bar{p} + e$ or $\bar{p} + \text{H}$. In fact, according to Ref. [14], the main decay channel of these states is radiative: emission of a photon with dissociation into $\bar{p} + \text{H}(1s)$. This information is based on a Born-Oppenheimer approach with the restrictive assumption that the hydrogen-atom subsystem is in a specific $n = 2$ state. This assumption is only partly in agreement with our results. A quantal three-body study of radiative transitions from quasibound to unbound states leading to this dissociation as well as of the electromagnetic deexcitations of the vibrational excited states will be the object of a future work.

-
- [1] M. Ahmadi, B. Alves, C. Baker, W. Bertsche, A. Capra, C. Carruth, C. Cesar, M. Charlton, S. Cohen, R. Collister, S. Eriksson, A. Evans, N. Evetts, J. Fajans, T. Friesen, M. Fujiwara, D. Gill, J. Hangst, W. Hardy, M. Hayden, C. Isaac, M. Johnson, J. Jones, S. Jones, S. Jonsell, A. Khramov, P. Knapp, L. Kurchaninov, N. Madsen, D. Maxwell, J. McKenna, S. Menary, T. Momose, J. Munich, K. Olchanski, A. Olin, P. Pusa, C. Rasmussen, F. Robicheaux, R. Sacramento, M. Sameed, E. Sarid, D. Silveira, G. Stutter, C. So, T. Tharp, R. Thompson, D. Van Der Werf, and J. Wurtele, *Nature* **557**, 71 (2018).
 - [2] W. A. Bertsche, E. Butler, M. Charlton, and N. Madsen, *J. Phys. B* **48**, 232001 (2015).
 - [3] B. R. Desai, *Phys. Rev.* **119**, 1385 (1960).
 - [4] N. Zurlo, M. Amoretti, C. Amsler, G. Bonomi, C. Carraro, C. L. Cesar, M. Charlton, M. Doser, A. Fontana, R. Funakoshi, P. Genova, R. S. Hayano, L. V. Jørgensen, A. Kellerbauer, V. Lagonarsino, R. Landua, E. Lodi Rizzini, M. Macrì, N. Madsen, G. Manuzio, D. Mitchard, P. Montagna, L. G. Posada, H. Pruys, C. Regenfus, A. Rotondi, G. Testera, D. P. Van der Werf, A. Variola, L. Venturelli, and Y. Yamazaki, *Hyperfine Interact.* **172**, 97 (2006).
 - [5] T. Yamazaki, N. Morita, R. S. Hayano, E. Widmann, and J. Eades, *Phys. Rep.* **366**, 183 (2002).
 - [6] M. Hori, A. Dax, J. Eades, K. Gomikawa, R. S. Hayano, N. Ono, W. Pirkel, E. Widmann, H. A. Torii, B. Juhász, D. Barna, and D. Horváth, *Phys. Rev. Lett.* **96**, 243401 (2006).
 - [7] M. Hori, H. Aghai-Khozani, A. Sótér, D. Barna, A. Dax, R. Hayano, T. Kobayashi, Y. Mu-

- rakami, K. Todoroki, H. Yamada, D. Horváth, and L. Venturelli, *Science* **354**, 610 (2016).
- [8] V. I. Korobov, D. Bakalov, and H. J. Monkhorst, *Phys. Rev. A* **59**, R919 (1999).
 - [9] Y. Kino, H. Kudo, and M. Kamimura, *Mod. Phys. Lett. A* **18**, 388 (2003).
 - [10] V. I. Korobov, L. Hilico, and J.-P. Karr, *Phys. Rev. A* **89**, 032511 (2014).
 - [11] V. I. Korobov, L. Hilico, and J.-P. Karr, *Hyperfine Interact.* **233**, 75 (2015).
 - [12] D. Baye, J. Dohet-Eraly, and P. Schoofs, *Phys. Rev. A* **99**, 022508 (2019).
 - [13] K. Sakimoto, *Phys. Rev. A* **90**, 032514 (2014).
 - [14] K. Sakimoto, *Phys. Rev. A* **98**, 042503 (2018).
 - [15] D. Baye and P.-H. Heenen, *J. Phys. A* **19**, 2041 (1986).
 - [16] M. Vincke, L. Malegat, and D. Baye, *J. Phys. B* **26**, 811 (1993).
 - [17] D. Baye, M. Hesse, and M. Vincke, *Phys. Rev. E* **65**, 026701 (2002).
 - [18] M. Hesse and D. Baye, *J. Phys. B* **32**, 5605 (1999).
 - [19] M. Hesse and D. Baye, *J. Phys. B* **36**, 139 (2003).
 - [20] D. Baye, *Phys. Rep.* **565**, 1 (2015).
 - [21] A. S. Coolidge and H. M. James, *Phys. Rev.* **51**, 855 (1937).
 - [22] C. L. Pekeris, *Phys. Rev.* **112**, 1649 (1958).
 - [23] Z. Zhen, *Phys. Rev. A* **41**, 87 (1990).
 - [24] M. Bollhöfer and Y. Notay, *Comput. Phys. Commun.* **177**, 951 (2007).
 - [25] J. E. Russell, *Phys. Rev. A* **1**, 721 (1970).
 - [26] R. F. Wallis, R. Herman, and H. W. Milnes, *J. Mol. Spectrosc.* **4**, 51 (1960).
 - [27] M. Vincke and D. Baye, *J. Phys. B* **39**, 2605 (2006).